The Solid Solutions $(Ce_{1-x}La_x)RuSn$

Oliver Niehaus[a], Bernard Chevalier[b], Paula M. Abdala[c], Florian Winter[a], and Rainer Pöttgen[a]

[a] Institut für Anorganische und Analytische Chemie and NRW Graduate School of Chemistry, Universität Münster, Corrensstraße 30, D-48149 Münster, Germany
[b] CNRS, Université de Bordeaux, ICMCB, 87 Avenue Dr. A. Schweitzer, F-33608 Pessac-Cedex, France
[c] SNBL at ESRF, European Synchrotron Radiation Facility, 6 Rue Jules Horowitz BP 220, Grenoble, France

Reprint requests to R. Pöttgen. E-mail: pottgen@uni-muenster.de

Z. Naturforsch. **2013**, *68b*, 1279 – 1287 / DOI: 10.5560/ZNB.2013-3257
Received September 17, 2013

X-Ray-pure samples of the solid solutions $(Ce_{1-x}La_x)RuSn$ were obtained up to $x = 0.5$. Powder diffraction data show the CeRuSn-type superstructure up to $x \approx 0.3$ and the CeCoAl-type subcell for higher lanthanum contents. The structure of a single crystal with $x = 0.5$ was refined on the basis of single-crystal X-ray diffractometer data: CeCoAl type, $C2/m$, $a = 1160.8(2)$, $b = 477.6(1)$, $c = 511.6(1)$ pm, $\beta = 102.97(2)^\circ$, $wR = 0.0510$, 444 F^2 values, 20 variables. Magnetic investigations were performed for all samples up to a lanthanum content of $x = 0.4$. No cooperative phenomena could be observed, and all samples show Curie-Weiss behavior above a certain temperature. The cerium valence is about 3.32(2) for all samples of the solid solution. Hence, La^{3+} has to replace Ce^{3+}as well as Ce^{4+} in a particular quantity. The electrical resistivity measurements confirm the suppression of the magnetic ordering and the structural transition upon replacement of cerium by lanthanum. ^{119}Sn Mössbauer spectra of samples with $x = 0.2$ and 0.5 are indicative of single tin sites with isomer shifts of $\delta = 1.86(1)$ mm s^{-1} for $x = 0.2$ and $\delta = 1.88(1)$ mm s^{-1} for $x = 0.5$. Both signals are subject to significant quadrupole splitting, a consequence of the low site symmetry. Results of XANES measurements are perfectly in line with the cerium valences determined by susceptibility measurements and yield a constant value of 3.16(1) for all investigated compounds.

Key words: Cerium, Stannide, Intermediate Valence

Introduction

The equiatomic intermetallic compounds Ce*TX* (*T* = electron-rich transition metal; *X* = element of the 3rd, 4th, or 5th main group) show a broad variety of different magnetic ground states depending on the crystal structure and the valence electron count. Most Ce*TX* compounds show antiferromagnetic ordering at low temperature but also a few ferromagnets have been observed. Very detailed studies were performed for the valence fluctuating compounds, *e. g.* CeRhGa [1], CeNiIn [2], CeRhIn [3], CeRhSn [4], or CeRhSb [5]. These intermetallics have only one crystallographic cerium site, leading to non-integer cerium valences over the whole temperature range.

The recently reported ternary stannide CeRuSn [6 – 13] shows more complicated valence behavior. At room temperature CeRuSn crystallizes with a superstructure of the monoclinic CeCoAl type with an ordering of trivalent and intermediate-valent cerium on distinct Wyckoff positions. The structure becomes incommensurate at low temperature. These structural changes have a strong influence on the magnetic and transport properties [8 – 13].

Besides investigations of changes in the structural and physical properties induced by temperature, we also started systematic studies of property changes in CeRuSn by substitution. Our first experiments concentrated on the solid solution $Ce(Ru_{1-x}Rh_x)Sn$ [14]. Upon small degrees of Ru/Rh substitution, the structure readily switches to the hexagonal ZrNiAl type of CeRhSn. Thus, ruthenium is inevitable for stabilization of the monoclinic structure. Herein we report on structural and property studies of the

Table 1. Lattice parameters of different samples of the solid solution $(Ce_{1-x}La_x)RuSn$.

Compound	a (pm)	b (pm)	c (pm)	β (deg)	V (nm^3)	Reference
CeRuSn	1156.1(4)	475.9(2)	1023.3(4)	102.89(3)	0.5488	[6]
CeRuSn	1155.3(1)	475.1(1)	1022.3(1)	102.96(1)	0.5468	this work
$(Ce_{0.95}La_{0.05})RuSn$	1156.4(1)	476.0(1)	1020.0(1)	103.01(1)	0.5470	this work
$(Ce_{0.9}La_{0.1})RuSn$	1156.5(1)	476.2(1)	1019.9(1)	103.11(1)	0.5470	this work
$(Ce_{0.85}La_{0.15})RuSn$	1156.8(1)	476.4(1)	1019.5(1)	103.06(1)	0.5473	this work
$(Ce_{0.8}La_{0.2})RuSn$	1157.5(1)	476.6(1)	1019.3(1)	103.11(1)	0.5477	this work
$(Ce_{0.75}La_{0.25})RuSn$	1158.0(1)	476.7(1)	1019.1(1)	103.05(1)	0.5480	this work
$(Ce_{0.7}La_{0.3})RuSn$	1158.2(1)	476.8(1)	1019.5(1)	103.08(1)	0.5484	this work
$(Ce_{0.65}La_{0.35})RuSn$	1158.6(1)	477.0(1)	510.4(1)	103.05(2)	0.2748	this work
$(Ce_{0.6}La_{0.4})RuSn$	1159.1(1)	477.2(1)	510.7(1)	103.02(1)	0.2752	this work
$(Ce_{0.5}La_{0.5})RuSn$	1160.8(1)	477.6(1)	511.6(1)	103.01(1)	0.2763	this work
$(Ce_{0.5}La_{0.5})RuSn$[a]	1160.8(2)	477.6(1)	511.6(1)	102.97(1)	0.2764	this work
$(Ce_{0.45}La_{0.55})RuSn$	1161.1(1)	477.3(1)	512.1(1)	102.92(1)	0.2766	this work
$(Ce_{0.4}La_{0.6})RuSn$	1162.7(1)	477.2(1)	513.1(1)	102.90(1)	0.2775	this work
$(Ce_{0.3}La_{0.7})RuSn$	1163.8(2)	476.9(1)	515.4(1)	102.91(1)	0.2788	this work

[a] Single crystal data.

solid solution $(Ce_{1-x}La_x)RuSn$, where lanthanum partially substitutes cerium in the CeRuSn-type structure.

Experimental

Synthesis

Starting materials for the syntheses of the $(Ce_{1-x}La_x)RuSn$ samples were sublimed lanthanum and cerium pieces (Sigma-Aldrich or smart elements, $> 99.9\,\%$), ruthenium powder (Allgemeine Pforzheim, $> 99.99\,\%$), and tin granules (Merck, $> 99.95\,\%$). Small pieces of lanthanum and cerium were first cut under dried (sodium wire) paraffin oil, washed with dried (sodium wire) *n*-hexane, and kept under argon in Schlenk tubes prior to the reactions. In a first step, lanthanum and cerium pieces were weighed in the desired atomic ratio (Table 1) and first arc-melted [15] under an argon atmosphere of *ca.* 700 mbar. The argon was purified over titanium sponge (900 K), silica gel, and molecular sieves. The $Ce_{1-x}La_x$ buttons were then mixed with appropriate amounts of ruthenium (cold-pressed as a pellet) and pieces of the tin granules. The elements were then arc-melted three times to ensure homogeneity. The resulting samples are stable in air over months. Small single crystals of these samples have metallic luster while ground polycrystalline powders are dark grey.

X-Ray diffraction

The polycrystalline $(Ce_{1-x}La_x)RuSn$ samples were characterized by Guinier patterns (imaging plate detector, Fujifilm BAS-1800) with Cu$K_{\alpha 1}$ radiation and α-quartz ($a = 491.30$ and $c = 540.45$ pm) as an internal standard. The monoclinic lattice parameters reported in Table 1 were obtained from standard least-squares fits. For the $x = 0.5$ sample we observed good agreement between the powder and single-crystal data.

Small single crystals were selected from the crushed $(Ce_{0.5}La_{0.5})RuSn$ sample. The crystals were glued to thin quartz fibers and first investigated by Laue photographs in a Buerger camera (white molybdenum radiation; imaging plate technique, Fujifilm, BAS-1800). Intensity data of a suitable crystal were collected at room temperature using a Stoe IPDS-II imaging plate diffractometer in oscillation mode (graphite-monochromatized MoK_α radiation). A numerical absorption correction was applied to the data set. Details about the data collection and the crystallographic parameters are summarized in Table 2.

Table 2. Crystal data and structure refinement for the compound $(Ce_{0.5}La_{0.5})RuSn$.

Empirical formula	$(Ce_{0.5}La_{0.5})RuSn$
Formula weight, g mol^{-1}	359.29
Unit cell dimensions, pm	Table 1
Space group; Z	$C12/m1$; 4
Pearson code	mS12
Calculated density, g cm^{-3}	8.63
Crystal size, μm^3	$10 \times 20 \times 20$
Absorption correction	numerical
Absorption coefficient, mm^{-1}	29.7
$F(000)$, e	606
θ range for data collection, deg	3.6 – 30
Range in *hkl*	± 16, ± 6, ± 7
Total no. of reflections	1415
Independent reflections / $R_{\rm int}$	444 / 0.0493
Reflections with $I > 3\,\sigma(I)$ / R_σ	275 / 0.0608
Data / parameters	444 / 20
Goodness-of-fit on F^2	1.04
$R1$ / $wR2$ for $I > 2\,\sigma(I)$	0.0244 / 0.0442
$R1$ / $wR2$ for all data	0.0591 / 0.0510
Extinction coefficient	12(5)
Largest diff. peak / hole, e Å^{-3}	2.62 / −3.00

Table 3. Atomic coordinates and anisotropic displacement parameters (pm^2) for the compound $(Ce_{0.5}La_{0.5})RuSn$. $U_{12} = U_{23} = 0$. U_{eq} is defined as one third of the trace of the orthogonalized U_{ij} tensor.

Atom	Wyckoff position	x	y	z	U_{11}	U_{22}	U_{33}	U_{13}	U_{eq}
Ce/La	4*i*	0.13090(8)	0	0.32182(17)	155(5)	113(3)	82(4)	43(3)	114(3)
Ru	4*i*	0.18965(12)	0	0.8460(4)	135(7)	74(5)	85(14)	121(8)	350(6)
Sn	4*i*	0.41425(9)	0	0.19261(19)	146(6)	74(4)	140(6)	45(4)	118(3)

Ce/La:	1	Ru	261.4	Ru:	1	Ce/La	261.4	Sn:	2	Ru	266.3
	1	Ru	267.1		2	Sn	266.3		1	Ru	280.5
	2	Ru	340.3		1	Ce/La	267.1		1	Sn	310.0
	2	Sn	342.3		1	Sn	280.5		1	Sn	332.3
	1	Sn	349.7		2	Ru	302.6		2	Ce/La	342.3
	2	Sn	350.5		2	Ce/La	340.3		1	Ce/La	349.7
	2	Sn	356.8		1	Ce/La	362.6		2	Ce/La	350.5
	1	Ru	362.6		2	Ce/La	356.8				
	2	Ce/La	379.6								
	1	Ce/La	387.9								
	1	Ce/La	394.8								

Table 4. Interatomic distances (pm), for the compound $(Ce_{0.5}La_{0.5})RuSn$ calculated with the powder lattice parameters. Standard deviations are equal or smaller than 0.2 pm. All distances of the first coordination spheres are listed.

Structure refinement

Careful examination of the data set showed only the small *C*-centered monoclinic subcell and no further systematic extinctions. As an example we present the *h3l* layer (Fig. 1) which was calculated from the data set integrated for the 2*c* superstructure. The diffraction data clearly show the breakdown of the superstructure. The atomic positions of CeCoAl [16], space group $C2/m$, were then taken as starting values, and the structure was refined using the JANA2006 package [17, 18] with anisotropic atomic displacement parameters (ADPs) for all atoms. In a separate refinement of the occupancy parameters no deviation from the ideal composition was observed. The 4*i* Ce/La site was refined with a fixed Ce : La ratio of 50 : 50. A final difference Fourier synthesis showed no significant residual peaks. The refined atomic positions, the ADPs, and the interatomic distances are given in Tables 3 and 4.

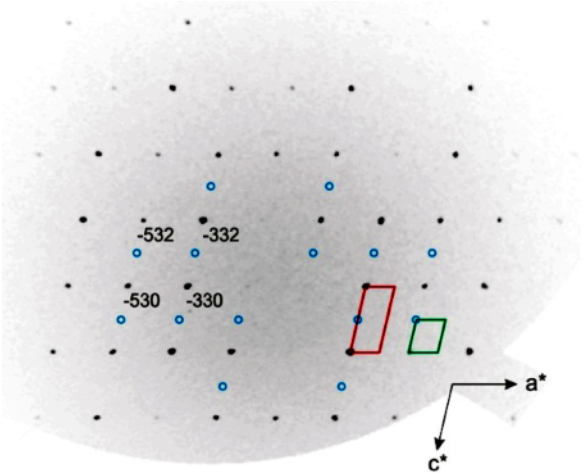

Fig. 1 (color online). The reciprocal layer *h3l* calculated from the diffractometer data set (integrated for the 2*c* superstructure cell). The unit cells of the subcell (red) and the superstructure (green) are given. Blue circles denote positions of (not detected) superstructure reflections.

Further details of the crystal structure investigation may be obtained from Fachinformationszentrum Karlsruhe, 76344 Eggenstein-Leopoldshafen, Germany (fax: +49-7247-808-666; e-mail: crysdata@fiz-karlsruhe.de, http://www.fiz-karlsruhe.de/request_for_deposited_data.html) on quoting the deposition number CSD-426673.

Magnetic susceptibility and electrical resistivity measurements

The magnetic susceptibility measurements were carried out on a Quantum Design Physical Property Measurement System (PPMS) using the VSM (Vibrating Sample Magnetometer) option. For the measurement approximately 20 mg pieces of single-phase samples were packed in kapton foil and attached to the sample holder rod. Magnetic investigations were performed in the temperature range of 2.5 to 305 K with magnetic flux densities up to 80 kOe ($1\,kOe = 7.96 \times 10^4\,A\,m^{-1}$).

The measurement of the electrical resistivity was carried out above 4.2 K on a bar of $0.5 \times 0.5 \times 3\,mm^3$ using a standard dc four probe method with silver paint contacts and an intensity current of 10 mA. Due to the presence of many pores and micro cracks in the samples, the absolute value of $\rho(T)$ could not be determined accurately; for this reason, the reduced resistivity $\rho(T)/\rho(270\,K)$ is reported here.

^{119}Sn Mössbauer spectroscopy

A $Ca^{119m}SnO_3$ source was available for the ^{119}Sn investigations, and a palladium foil of 0.05 mm thickness was used to reduce the tin *K* X-rays concurrently emitted by this source. The measurements of the $(Ce_{0.5}La_{0.5})RuSn$ and $(Ce_{0.8}La_{0.2})RuSn$ samples were performed in the usual transmission geometry at room temperature. The samples were placed within a thin-walled PMMA container at a thickness corresponding to about 10 mg Sn cm^{-2}. Spectra were fitted with the NORMOS-90 program system [19].

XANES – X-ray absorption near edge structure

X-Ray absorption spectra at the CeL_{III} edge were collected at BM01-B (Swiss Norwegian Beamlines, SNBL) at the European Synchrotron Radiation Facility (ESRF), Grenoble, France. The electron energy in the storage ring was 6 GeV with a maximum current of 200 mA. The measurements were performed in transmission mode using a Si (111) double crystal monochromator. The second crystal of the monochromator was detuned by 60 % in order to suppress higher harmonic radiation. The intensities of the incident and transmitted X-rays were monitored with nitrogen- and helium-filled ionization chambers. All spectra were acquired in a continuous scanning mode from 5680 to 5874 eV, with energy steps of 0.3 eV for 15 min each scan.

The samples, after being grounded in an agate mortar using cyclohexane to avoid oxidation, were homogeneously mixed with cellulose powder (Sigma-Aldrich) in order to optimize the edge jump and pressed into pellets. Measurements were performed at ambient conditions. Data were recorded with $Ce_2(CO_3)_3$ or CeO_2 as trivalent and tetravalent cerium reference compounds, respectively. The ATHENA software was used for processing and fitting of the data.

Results and Discussion

Crystal chemistry and course of the solid solutions

The ternary stannide CeRuSn crystallizes with its own peculiar crystal structure, space group $C2/m$ [6]. At room temperature the structure can be considered as a superstructure of the monoclinic CeCoAl type, resulting from an *isomorphic* symmetry reduction of index 2, paralleled by a doubling of the *c* lattice parameter. For a detailed crystal-chemical discussion we refer to our previous studies [6 – 9]. Herein we focus only on the differences in the cerium coordination in the superstructure and the solid solution $(Ce_{1-x}La_x)RuSn$. The corresponding near-neighbor co-ordinations are presented in Fig. 2.

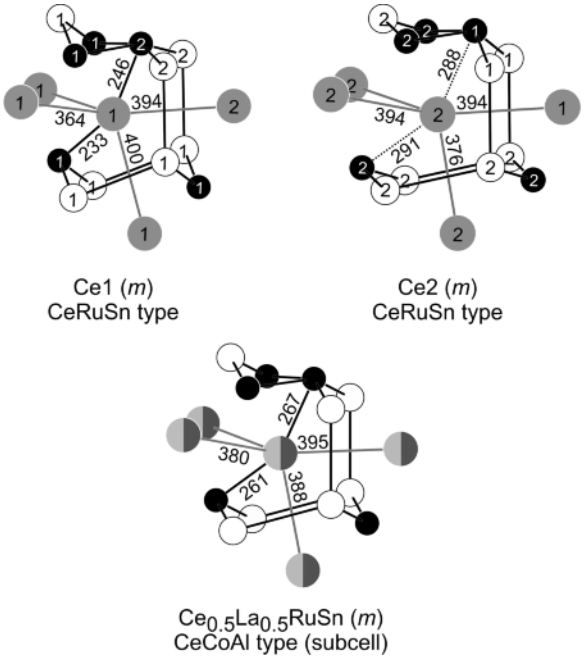

Fig. 2. Coordination of the cerium atoms in the CeRuSn structure (top) and the CeCoAl-type subcell for $(Ce_{0.5}La_{0.5})RuSn$ (bottom). Cerium, ruthenium and tin atoms are drawn as medium grey, black filled and open circles, respectively. The mixed-occupied Ce/La site is shaded. Relevant interatomic distances (pm) and site symmetries (in parentheses) are given.

The ordering of trivalent and intermediate-valent (almost tetravalent) cerium in CeRuSn causes severe differences in the interatomic distances. The Ce2 atoms are trivalent with Ce2–Ru distances of 288 and 291 pm, in close agreement with the sum of the covalent radii of 289 pm [20]. This is different for the Ce1 atoms. The smaller effective size of almost tetravalent Ce1 leads to drastically shortened Ce1–Ru distances of 233 and 246 pm, also observed in many intermetallics based on Ce and Ru [21, 22]. These are a consequence of strong covalent Ce1–Ru bonding [7], the strongest bonding interactions in the CeRuSn structure. Also the Ce–Ce distances are affected by the differing Ce–Ru bonding: Ce1–Ce1 = 364 and 400 pm *vs.* Ce2–Ce2 = 394 and 376 pm (Fig. 2).

The important question for the solid solutions $(Ce_{1-x}La_x)RuSn$ concerns the cerium site occupancies. Since cerium and lanthanum differ only by one electron, even high-quality single-crystal X-ray data will not help to answer this question undoubtedly. Thus

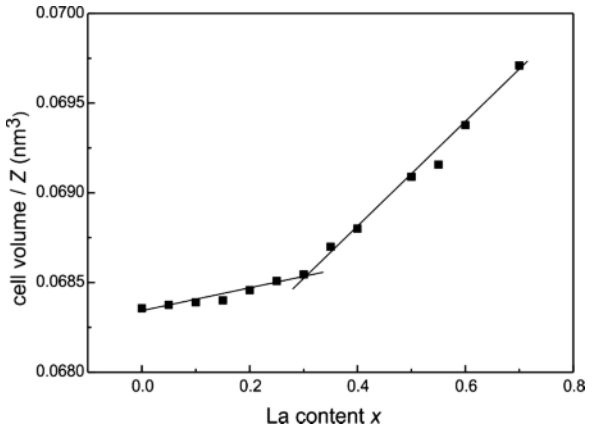

Fig. 3. Course of the unit cell volume in the solid solution $(Ce_{1-x}La_x)RuSn$. The solid lines serve as a guide to the eye.

our discussion relies on the course of the lattice parameters and single-crystal data of the $(Ce_{0.5}La_{0.5})RuSn$ compound with a fixed ratio of Ce : La. Substitution of cerium by lanthanum leads to a small increase of the cell volume up to $x \approx 0.3$ (Fig. 3). This is understandable in view of the slightly larger size of the lanthanum atoms. Careful inspection of the Guinier powder patterns for the samples up to $x \approx 0.3$ still showed weak superstructure reflections. Samples from $x \approx 0.3$ up to $x = 0.7$ show only the subcell, and the increase of the cell volume is much more pronounced (Fig. 3 and Table 1). One might speculate that the La atoms preferably substitute on the trivalent Ce2 site and from $x \approx 0.3$ La also substitutes the Ce1 sites which leads to longer La^{III}–Ru distances (as compared to $Ce^{\sim IV}$–Ru). Taking the magnetization measurements into account, no preferred substitution can be predicted which will be discussed later. The subcell structure is only stable up to $x \approx 0.7$. Higher lanthanum content leads to other phases. Our phase-analytical studies gave no hint for a pure equiatomic sample with composition LaRuSn.

Although the single-crystal data do not allow for Ce/La distinction, we can examine the influence on the average Ce/La–Ru distances. As is evident from Fig. 2, we observe Ce/La–Ru distances of 261 and 267 pm, more or less in between the data for Ce1 and Ce2 in the superstructure (Table 4). The same holds true for the Ce–Ce distances. A strong hint for still existing short Ce–Ru distances (at least in small domains) is the strongly enhanced U_{33} parameter for the Ru atoms. This is exactly the direction in which the ruthenium atoms show the highest shifts in the atomic parameters upon formation of the superstructure.

Magnetic susceptibility data

Magnetic investigations were performed for all samples up to a lanthanum content of $x = 0.4$. Figs. 4 and 5 display the temperature dependence of the magnetic susceptibility and its reciprocal (χ and χ^{-1} data) of $(Ce_{0.9}La_{0.1})RuSn$ and $(Ce_{0.6}La_{0.4})RuSn$ compounds measured with a magnetic field of 10 kOe. To compare the magnetic behavior the reciprocal susceptibility of all samples is shown in Fig. 6. No cooperative phenomena could be observed for any compound. Susceptibility measurements of $(Ce_{0.95}La_{0.05})RuSn$ (not shown here) have proven that five percent of lanthanum is already enough to suppress the hysteresis that occurs for pure CeRuSn [6]. $(Ce_{0.9}La_{0.1})RuSn$

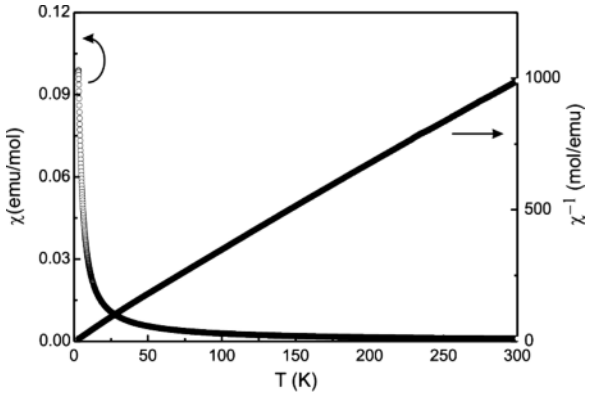

Fig. 4. Temperature dependence of the magnetic susceptibility (χ and χ^{-1} data) for the compound $(Ce_{0.9}La_{0.1})RuSn$.

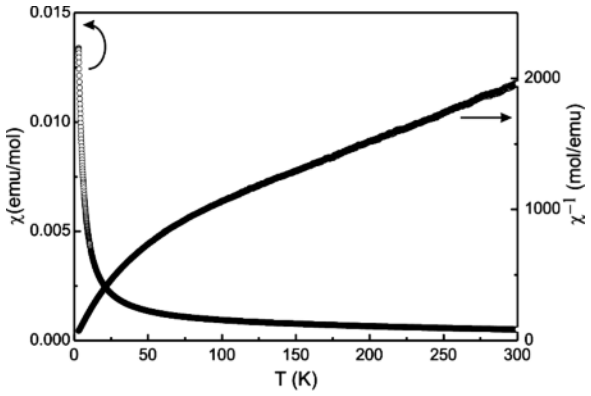

Fig. 5. Temperature dependence of the magnetic susceptibility (χ and χ^{-1} data) for the compound $(Ce_{0.6}La_{0.4})RuSn$.

Table 5. Data of the magnetic measurements of different compounds of the solid solution $(Ce_{1-x}La_x)RuSn$. C: Curie constant; θ: paramagnetic Curie temperature; μ_{exp}: experimental magnetic moment.

Compound	C (emu K per f. u.)	C (emu K per Ce atom)	Θ (K)	μ_{exp} per Ce atom	Reference
CeRuSn	0.38(2)	0.38	–	1.74	[6]
$(Ce_{0.95}La_{0.05})RuSn$	0.379(1)	0.399	−30	1.78	this work
$(Ce_{0.9}La_{0.1})RuSn$	0.340(1)	0.378	−5	1.74	this work
$(Ce_{0.85}La_{0.15})RuSn$	0.331(1)	0.389	−115	1.77	this work
$(Ce_{0.8}La_{0.2})RuSn$	0.305(1)	0.381	−139	1.75	this work
$(Ce_{0.75}La_{0.25})RuSn$	0.273(1)	0.364	−44	1.71	this work
$(Ce_{0.7}La_{0.3})RuSn$	0.260(1)	0.371	−196	1.72	this work
$(Ce_{0.65}La_{0.35})RuSn$	0.254(1)	0.391	−110	1.77	this work
$(Ce_{0.6}La_{0.4})RuSn$	0.219(1)	0.362	−134	1.71	this work

shows Curie-Weiss behavior over the whole temperature range (Fig. 4). However, the reciprocal magnetic susceptibility of $(Ce_{0.6}La_{0.4})RuSn$ exhibits a linear temperature dependence only above 100 K (Fig. 5). Deviations from the Curie-Weiss law can be observed for all compounds with a higher lanthanum content than $x = 0.1$ (Fig. 6) and are, most likely, related to crystal field effects (CEF). In a hexagonal symmetry, for example, the Ce $^2F_{5/2}$ state is split into three doublets [23 – 25]. No relationship between the lanthanum content and the magnetic field splitting could be observed. Due to this fact no fitting of the different magnetic states has been performed.

Table 5 presents the fitting results for all investigated compounds with the Curie-Weiss law. These results, as well as Fig. 6, clearly indicate an increase of the reciprocal magnetic susceptibility with higher lanthanum contents. Calculations of the Curie constants as a function of the cerium content prove intermediate valence

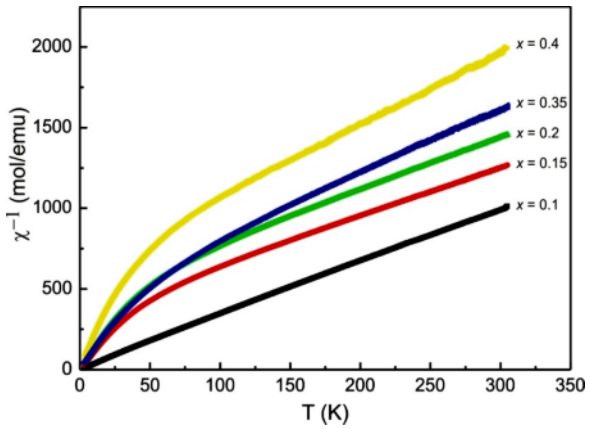

Fig. 6 (color online). Temperature dependence of the reciprocal magnetic susceptibilities (χ^{-1}) for various $(Ce_{1-x}La_x)RuSn$ compounds.

behavior, however, without pronounced changes. Because of the two different cerium sites in the CeRuSn-type structure, it is not easy to calculate the magnetic moment or the accurate cerium valences.

$(Ce_{0.6}La_{0.4})RuSn$ crystallizes in the CeCoAl-type structure and exhibits only one cerium site. Accordingly, the cerium valence can definitely be calculated by comparison of the determined effective magnetic moment with the theoretical one. Fitting the susceptibility measurement of $(Ce_{0.6}La_{0.4})RuSn$ with a Curie-Weiss law yields a Curie constant of $C_m = 0.36\,\text{emu} * \text{K/mol}$ and an effective magnetic moment $\mu_{eff} = 1.71\,\mu_B\,\text{mol}^{-1}$ ($\mu_{eff} = (8C_m)^{1/2}$). In comparison with the theoretical effective magnetic moment of $2.54\,\mu_B\,\text{mol}^{-1}$ for a free Ce^{3+} ion a cerium valence of about 3.33(2) can be assumed for $(Ce_{0.6}La_{0.4})RuSn$.

The results of the magnetic measurements suggest that no cerium site is substituted preferably by lanthanum atoms because of the overall constant cerium valence. If the trivalent Ce2 site would be substituted at first, a higher amount of Ce^{4+} should be observed. The continuous substitution of lanthanum on the Ce1 site causes weaker Ce1-Ru interactions, which lead to the breakdown of the CeRuSn superstructure.

Electrical resistivity

The temperature dependence of the reduced electrical resistivity $\rho(T)/\rho(270\,\text{K})$ of the $(Ce_{1-x}La_x)RuSn$ compounds with $x = 0.25$ and 0.40 reveals several characteristics (Fig. 7): (i) between 270 and 25 K, $\rho(T)/\rho(270\,\text{K})$ decreases but reveals a downward curvature; such behavior is expected for Kondo-type interactions in the presence of crystal field effects as observed for many compounds based on cerium [26]; (ii) below 25 K, $\rho(T)/\rho(270\,\text{K})$ increases

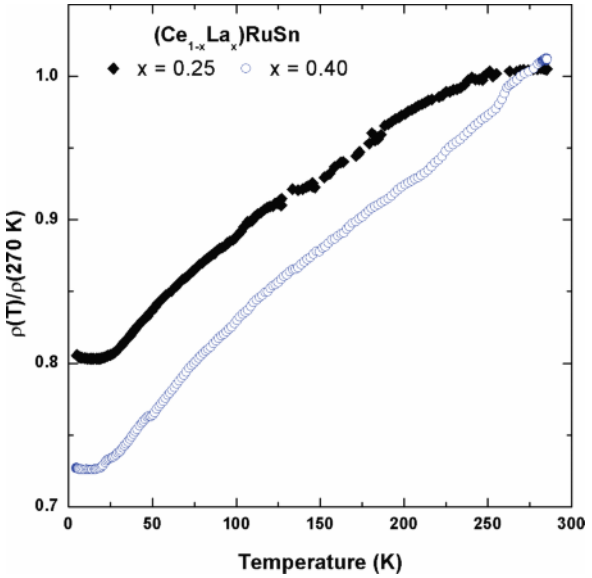

Fig. 7 (color online). Temperature dependence of the reduced electrical resistivity for various $(Ce_{1-x}La_x)RuSn$ compounds with $x = 0.25$ and 0.40.

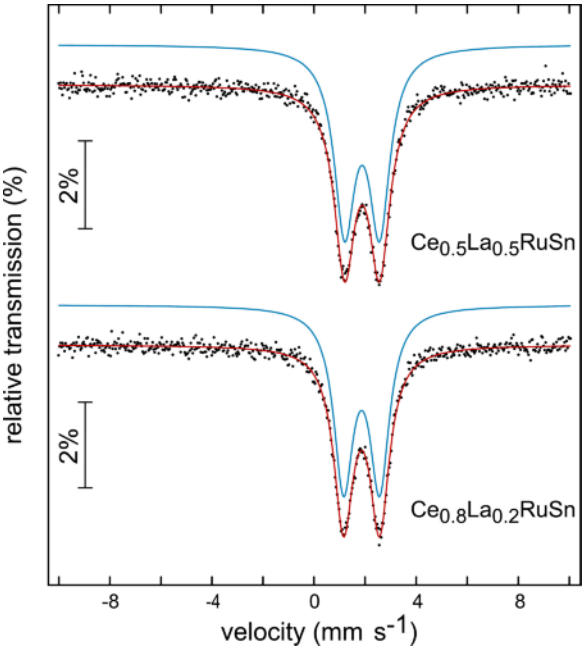

Fig. 8 (color online). Experimental and simulated ^{119}Sn Mössbauer spectra of $(Ce_{0.5}La_{0.5})RuSn$ and $(Ce_{0.8}La_{0.2})RuSn$ at room temperature.

slowly for $(Ce_{0.75}La_{0.25})RuSn$ but tends to saturate for $(Ce_{0.6}La_{0.4})RuSn$. The latter behaviors suggest that the Kondo effect is more influential for the compound $(Ce_{0.75}La_{0.25})RuSn$ containing more cerium.

It is interesting to note that the value of $\rho(T) = \rho(270\,\mathrm{K})$ determined at 4.2 K is smaller for $(Ce_{0.6}La_{0.4})RuSn$ than for $(Ce_{0.75}La_{0.25})RuSn$ indicating an increase of the metallic behavior in the solid solution following an increase of the lanthanum content. Finally, these curves reveal no anomaly as observed for CeRuSn [8] confirming the absence of magnetic ordering and of structural transition when lanthanum replaces cerium in CeRuSn. This agrees with the magnetization measurements.

^{119}Sn Mössbauer spectroscopy

Fig. 8 shows the room-temperature ^{119}Sn Mössbauer spectra of $(Ce_{1-x}La_x)RuSn$ samples with $x = 0.2$ and 0.5. Both spectra could be well reproduced with single tin sites with isomer shifts of $\delta = 1.86(1)\,\mathrm{mm\,s^{-1}}$ for $x = 0.2$ and $\delta = 1.88(1)\,\mathrm{mm\,s^{-1}}$ for $x = 0.5$. Both signals are subject to significant quadrupole splitting of $\Delta E_Q = 1.41(1)\,\mathrm{mm\,s^{-1}}$ for $x = 0.2$ and $\Delta E_Q = 1.37(1)\,\mathrm{mm\,s^{-1}}$ for $x = 0.5$. The experimental line width parameters are $\Gamma = 0.93(1)\,\mathrm{mm\,s^{-1}}$ for $x = 0.2$ and $\Gamma = 0.99(1)\,\mathrm{mm\,s^{-1}}$ for $x = 0.5$. Thus, also the ^{119}Sn spectra point to the subcell structure. In contrast, the spectra of pure CeRuSn [11] show a superposition of two sub-spectra of the two crystallographically independent tin sites. The experimental line widths of the $x = 0.2$ and 0.5 samples are only slightly enhanced. This might be a consequence of domains with slightly differing compositions, since we deal with samples from solid solution with statistical Ce/La occupancy.

XANES – X-ray absorption near edge structure

As already proven for the solid solution $Ce(Rh_{1-x}Ru_x)Sn$, X-ray absorption spectroscopy (XAS) at the CeL_{III} edge is to be considered a powerful tool for studying the valence state in cerium compounds [14]. XANES gives a relevant representation of the electronic configuration yielding the $4f$ occupation number. In the ground state of the mixed-valence compounds, the energies of Ce $4f^0$ and $4f^1$ configurations are located close to each other and mixed by the hybridization between the $4f$ and conduction band states. In the final state of the CeL_{III}

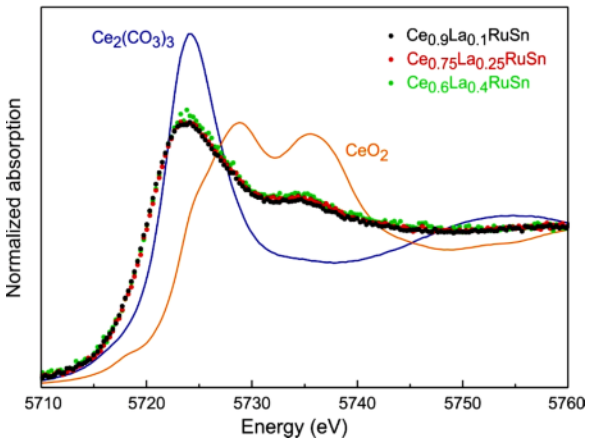

Fig. 9 (color online). Normalized L_{III} XANES spectra of $(Ce_{1-x}La_x)RuSn$ ($x = 0.1$, 0.25 and 0.4) plotted together with $Ce_2(CO_3)_3$ and CeO_2 as reference compounds.

XAS spectrum, the energies of the two configurations are assumed to be separated by a strong core-hole potential ($\sim$ 10 eV) on the $4f$ state. The spectrum exhibits a characteristic double-peak profile that is considered as an evidence of the mixed valence state. Assuming that the L_{III} absorption is a single-particle process and neglecting final state effects, the intensity ratio of the two peaks can be used for an estimation of the averaged valence number.

The normalized Ce L_{III}-edge XANES spectra for the $(Ce_{1-x}La_x)RuSn$ solid solutions are presented in Fig. 9. The spectra of the references CeO_2 and $Ce_2(CO_3)_3$ have been plotted for comparison. The XANES spectra were similar for all samples, exhibiting the characteristic double-bump feature for mixed valency. The main 'white line' at the energy of 5724 eV can be attributed to the final state configuration of Ce^{3+}, and the shoulder observed at the energy of 10 – 10.1 eV above the main white line can be ascribed to the Ce^{4+} electronic configuration.

Table 6. Energy difference (ΔE) between the Ce^{3+} and Ce^{4+} peak and the estimated average cerium valence for $(Ce_{1-x}La_x)RuSn$ ($x = 0.1$, 0.25 and 0.4) determined by fitting of the XANES spectra.

Compound	ΔE (eV)	Average Ce valence
$(Ce_{0.9}La_{0.1})RuSn$	10.0	3.15(2)
$(Ce_{0.75}La_{0.25})RuSn$	10.1	3.16(2)
$(Ce_{0.6}La_{0.4})RuSn$	10.1	3.16(2)

The XANES spectra were fitted by a least-squares procedure using a simplified model that contains two arctangent functions to describe the transitions into the continuum states and two Lorentzian functions to take into account the $4f$ states. Because there is a high overlap of these functions, the fittings were performed by carefully varying the parameters that define the Lorentzians and arctangent functions.

The values of the average valence are listed in Table 6. Within the standard deviation the cerium valence is constant for all investigated compounds, which is perfectly in line with the results of the susceptibility measurements (*vide supra*). Consequently, no influence of the lanthanum content on the cerium valence can be observed. Considering that the cerium valence in CeO_2 determined by XANES is only about 3.5 [27], the absolute value of 3.16(2) agrees very well with the value of 3.33(2) obtained by susceptibility measurements for $(Ce_{0.6}La_{0.4})RuSn$. Since both methods prove a constant cerium valence, a value of 3.32(2) results for all compounds by magnetic susceptibility measurements.

Acknowledgement

We thank Dipl.-Ing. U. Ch. Rodewald for the data collection. This work was supported by the Deutsche Forschungsgemeinschaft. O. N. is indebted to the NRW Forschungsschule *Molecules and Materials – A common Design Principle* for a PhD stipend.

[1] J. Goraus, A. Ślebarski, M. Fijałkowski, *J. Alloys Compd.* **2011**, *509*, 3735.
[2] H. Fujii, T. Inoue, Y. Andoh, T. Takabatake, K. Satoh, Y. Maeno, T. Fujita, J. Sakurai, Y. Yamaguchi, *Phys. Rev. B* **1989**, *39*, 6840.
[3] D. T. Adroja, S. K. Malik, B. D. Padalia, R. Vijayaraghavan, *Phys. Rev. B* **1989**, *39*, 4831.
[4] A. Ślebarski, M. B. Maple, E. J. Freeman, C. Sirvent, M. Radlowska, A. Jezierski, E. Granado, Q. Huang, J. W. Lynn, *Phil. Mag. B* **2002**, *82*, 943.
[5] S. K. Malik, D. T. Adroja, *Phys. Rev. B* **1991**, *43*, 6277.
[6] J. F. Riecken, W. Hermes, B. Chevalier, R.-D. Hoffmann, F. M. Schappacher, R. Pöttgen, *Z. Anorg. Allg. Chem.* **2007**, *633*, 1094.

[7] S. F. Matar, J. F. Riecken, B. Chevalier, R. Pöttgen, V. Eyert, *Phys. Rev. B* **2007**, *76*, 174434.
[8] J. A. Mydosh, A. M. Strydom, M. Baenitz, B. Chevalier, W. Hermes, B. Chevalier, *Phys. Rev. B* **2011**, *83*, 054411.
[9] R. Feyerherm, E. Dudzik, S. Valencia, J. A. Mydosh, Y.-K. Huang, W. Hermes, R. Pöttgen, *Phys. Rev. B* **2012**, *85*, 085120.
[10] J. Fikáček, J. Prokleška, M. Míšek, J. Custers, S. Daniš, J. Prchal, V. Sechovský, I. Císařová, *Phys. Rev. B* **2012**, *86*, 054108.
[11] F. M. Schappacher, P. Khuntia, A. K. Rajarajan, M. Baenitz, J. A. Mydosh, B. Chevalier, S. F. Matar, R. Pöttgen, *Z. Naturforsch.* **2012**, *67b*, 473.
[12] J. Fikáček, J. Prchal, J. Prokleška, I. Císařová, V. Sechovský, *Solid State Phen.* **2013**, *194*, 40.
[13] K. Prokeš, J. Mydosh, O. Prokhnenko, W.-D. Stein, S. Landsgesell, W. Hermes, R. Feyerherm, R. Pöttgen, *Phys. Rev. B* **2013**, *87*, 094421.
[14] O. Niehaus, P. M. Abdala, J. F. Riecken, F. Winter, B. Chevalier, R. Pöttgen, *Z. Naturforsch.* **2013**, *68b*, 960.
[15] R. Pöttgen, Th. Gulden, A. Simon, *GIT Labor-Fachzeitschrift* **1999**, *43*, 133.
[16] Yu. N. Grin, O. M. Sichevich, V. A. Bruskov, R. M. Rykhal', Ya. P. Yarmolyuk, *Sov. Phys. Crystallogr.* **1983**, *28*, 346.
[17] V. Petříček, M. Dušek, L. Palatinus, JANA2006, The Crystallographic Computing System, Institute of Physics, University of Prague, Prague (Czech Republic) **2006**.
[18] L. Palatinus, G. Chapuis, *J. Appl. Crystallogr.* **2007**, *40*, 786.
[19] R. A. Brand, NORMOS, Mössbauer fitting Program, University of Duisburg, Duisburg (Germany) **2002**.
[20] J. Emsley, *The Elements*, Oxford University Press, Oxford **1999**.
[21] W. Hermes, S. F. Matar, R. Pöttgen, *Z. Naturforsch.* **2009**, *64b*, 901.
[22] T. Mishra, R.-D. Hoffmann, C. Schwickert, R. Pöttgen, *Z. Naturforsch.* **2011**, *66b*, 771.
[23] H. Kitazawa, C. Schank, S. Thies, B. Seidel, C. Geibel, F. Steglich, *J. Phys. Soc. Jpn.* **1992**, *61*, 1461.
[24] B. Chevalier, B. Heying, U. Ch. Rodewald, C. P. Sebastian, E. Bauer, R. Pöttgen, *Chem. Mater.* **2007**, *19*, 3052.
[25] W. Hermes, B. Chevalier, U. Ch. Rodewald, S. F. Matar, F. Weill, I. Schellenberg, R. Pöttgen, H. Lueken, M. Speldrich, *Chem. Mater.* **2011**, *23*, 1096.
[26] B. Cornut, B. Coqblin, *Phys. Rev. B* **1972**, *5*, 4541.
[27] R. Niewa, Z. Hu, C. Grazioli, U. Rößler, M. S. Golden, M. Knupfer, J. Fink, H. Giefers, G. Wortmann, F. M. F. de Groot, F. J. DiSalvo, *J. Alloys Compd.* **2002**, *346*, 129.